



HAL
open science

Coupled modeling of cement/ claystone interactions and radionuclides migration

Laurent de Windt, Delphine Pellegrini, Jan van Der Lee

► **To cite this version:**

Laurent de Windt, Delphine Pellegrini, Jan van Der Lee. Coupled modeling of cement/ claystone interactions and radionuclides migration. *Journal of Contaminant Hydrology*, 2004, 68, pp.165-182. hal-00596549

HAL Id: hal-00596549

<https://minesparis-psl.hal.science/hal-00596549>

Submitted on 4 Nov 2015

HAL is a multi-disciplinary open access archive for the deposit and dissemination of scientific research documents, whether they are published or not. The documents may come from teaching and research institutions in France or abroad, or from public or private research centers.

L'archive ouverte pluridisciplinaire **HAL**, est destinée au dépôt et à la diffusion de documents scientifiques de niveau recherche, publiés ou non, émanant des établissements d'enseignement et de recherche français ou étrangers, des laboratoires publics ou privés.

Coupled modeling of cement/claystone interactions and radionuclide migration

L. De Windt^{a,*}, D. Pellegrini^b, J. van der Lee^a

^a*Ecole des Mines de Paris, Centre d'Informatique Géologique,
35 R. St-Honoré, 77300 Fontainebleau, France.*

^b*Institut de Radioprotection et de Sûreté Nucléaire, DES/SESID,
BP 17, 92262 Fontenay-aux-Roses cedex, France.*

* **Corresponding author.** Email: dewindt@cig.ensmp.fr, Fax:+33-1-64694713.

Abstract

The interactions between cement and a clayey host-rock of an underground repository for intermediate-level radioactive waste are studied with the reactive transport code HYTEC for supporting performance assessment. Care is taken to use relevant time scales (100,000 years) and dimensions. Based on a literature review, three hypotheses are considered with respect to the mineralogical composition of the claystone and the neo-formed phases. In the long term, the pH is buffered for all hypotheses and important mineral transformations occur both in cement and the host-rock. The destruction of the primary minerals is localized close to the cement/claystone interface and is characterized by the precipitation of secondary phases with retention properties (illite, zeolite). However, beyond the zone of intense mineral transformations, the pore water chemistry is also disturbed over a dozen meters due to an attenuated but continuous flux of hydroxyl, potassium and calcium ions. Four interdependent mechanisms control the pH profile in the whole system: diffusion of the alkaline plume, mineralogical buffering, ion exchange and clogging of the pore space at the cement/claystone interface. The migration of a selected group of radionuclides (Cs, Ra, Tc and U) is explicitly integrated in the simulations of the strongly coupled system. Theoretical profiles of distribution coefficient (Kd) and solubility limit values are derived from the simulations, and their sensitivity with respect to the system evolution is estimated.

Key words: cement, clay, radioactive waste, radionuclide migration, reactive transport.

* Corresponding author. Email: dewindt@cig.ensmp.fr

1 Context and objectives

Argillaceous media are being investigated in several countries as one of the geological formations that could possibly host an underground repository for radioactive waste due notably to their favorable hydraulic and chemical containment properties. Design options of disposal facilities may include large amounts of cementitious material for waste immobilization, for minimizing corrosion and radionuclide migration and for supporting cavities such as drifts and vaults. For purposes of safety assessment, these positive features have to be balanced against the potentially negative effects of cement degradation on the performance of the geological barrier in the near-field. The pore water chemistry of most cements is characterized by high amounts of alkaline and hydroxyl ions ($\text{pH} \geq 13$). The migration of the cement pore water into the surrounding media leads to the formation of an alkaline plume. Accordingly, local destruction of minerals constitutive of the host-rock can occur as well as a substantial modification of the hydraulic and retention properties of host-rock in near-field.

Performance assessment of radioactive waste disposal requires to model long-term migration of radionuclides through the engineered barriers and the geological environment since the considered time scales, of several thousands of years, are out of range of any direct experiments. Such integrated transport modeling addresses the most significant features and processes at scales representative of the disposal site but usually requires a simplified representation of the later. Hence, geochemical and hydrodynamic processes are usually accounted for in an independent manner. The chemical complexity is reduced to distribution coefficients (Kd) and solubility limits (SL) that are assigned to components of the repository. These input parameters are generally assumed to be constant in time, although the components may be progressively disturbed by the waste degradation and the geochemical interaction between engineered barriers and the geological medium (Sagar et al., 2002; Savage, 1994).

Considerable progress has been made in the field of reactive transport models and computer codes which offer the possibility of simulating geochemically complex systems in a hydrodynamic context (van der Lee and De Windt, 2001). This type of process level modeling can provide essential information to integrated performance assessment regarding the potential evolution of the near-field geochemistry, the relevance and coupling of processes, the interpretation of radionuclide containment at a mechanistic level and the estimation of Kd and SL value evolution in time and space. It therefore provides direct information for assessing the pros and cons of engineered barriers with regard to radionuclide migration and allows backing up the simplifications made in PA modeling.

In this respect, a rigorous model has been developed using the reactive transport code HYTEC to assess the geochemical evolution of an argillaceous host-rock due to interactions with cementitious waste and backfill materials. The considered system is an underground disposal for intermediate level radioactive waste (ILW) in stiff clay. Care has been taken to use design hypotheses and time scales consistent with the repository projects developed to date. Based on a literature review, the sensitivity of the system evolution is assessed with respect to the variability of the experimental results. The impact of precipitation and dissolution of minerals on porosity and diffusion is studied, illustrating how both hydrological and chemical processes occur interdependently. At last, simulation of Cs migration within the coupled evolving system, together with the derivation of Kd and SL values for Cs, Ra, Tc and U, enable some evaluation of the consequences of geochemical evolutions in near-field on the containment properties of the repository. These radionuclides have been selected mainly on the basis of data availability and interest for safety. Actually, they are present in ILW but also in spent fuel, which disposal may include a cementitious engineered barrier as well, and they contribute to the dosimetric impact especially for the spent fuel case. This selection of radionuclides is thus studied as an example that is safety relevant, but should however not be considered here as the hierarchy of the radionuclides to be treated in priority with respect to safety issues.

2 Model assumptions and thermodynamic data

2.1 Site and model features

The studied system is a simplified representation of the near-field of an ILW repository in a deep argillaceous formation, derived from the various repository designs studied at present time. The host-rock formation properties are those of stiff clays such as can be found in France and Switzerland (De Windt et al., 1999): a strongly indurated claystone and with a low porosity. Diffusion is the predominant migration mechanism. The hydrogeological parameters are provided in Table 1. Identical parameters for anionic and cationic species were used in the reactive transport code (HYTEC, see below), which is a simplification for clayey materials when considering partial anion exclusion may occur in the smallest pores. Waste disposal design comprises horizontal tunnels perpendicular to handling drifts. The tunnels are 100 m long, 6 m in diameter and 26 m apart (see Figure 1). The nuclear waste is immobilized in a cementitious matrix. The cylindrical containers (1 m in diameter) are aligned in 4 rows in each tunnel. It is assumed that the tunnels are entirely filled with cement, i.e. the same type of cement is used for the waste and the engineered barrier. An ordinary Portland cement (OPC) is considered, of which porosity

and diffusion coefficients are detailed in Table 1. In accordance with field observations (Cabrera et al., 1999), an excavation damaged zone (EDZ) is defined around the tunnels as a strongly fractured zone (EDZ-I, 1 m thick) and a disturbed transition zone (EDZ-II, 1.5 m thick), with higher porosities and pore diffusion coefficients than the undisturbed clayey rock (see Table 1). The temperature is 20 °C, representative of thermal conditions prevailing in host-rock since ILW waste does not generate significant thermal output.

In our study, the OPC interstitial water is a K-Na-OH fluid in equilibrium with portlandite (25% weight), ettringite (15%) and a calcium silicate hydrate with a Ca/Si ratio of 1.8 (60%). The ionic strength is about 0.22 and the pH value is 13.3 at 20 °C. In the calculations, the cement was considered as a reactive geochemical zone in itself and not as a constant boundary condition. The argillaceous rock is a claystone with high contents in clay minerals, mainly illite (22% weight) and interstratified illite/smectite (28%). Quartz (30%), calcite (15%), dolomite (3%), pyrite (1%) and organic matter (1%) are also present. The organic matter was assumed to be mature, i.e. non reactive, and therefore was not taken into account in the simulations. In our model, Ca-montmorillonite represents the smectitic part of the claystone. The pore water has a pH of 7.7 with sodium, chloride and sulfate as major ions; its ionic strength is about 0.075. The cation exchange capacity (CEC) is 20 meq/100g of rock, Ca being the dominant exchangeable cation: Ca (77%, in equivalent fraction), Na (19%), Mg (3.5%), K (0.5%). At the in-situ pH, the exchangeable proton concentration was estimated to be close to 10 % of the CEC as in Cranga et al. (1998). The pore water is in equilibrium with the minerals and the exchangeable ions related to the clay minerals.

The reactive transport code HYTEC (van der Lee et al., 2003), based on the geochemical code CHESS, was used to simulate the cement-claystone interaction processes. HYTEC simulates advective, dispersive and diffusive transport for solutes and colloids using a finite element approach. A wide range of processes such as aqueous chemistry, redox, dissolution/precipitation, surface complexation and ion exchange can be modeled at equilibrium or with kinetic control. In HYTEC, transport is coupled to chemistry according to:

$$\frac{\partial \omega c_i}{\partial t} = \nabla(D \cdot \nabla c_i) - \nabla(c_i U) - \frac{\partial \omega \bar{c}_i}{\partial t}, \quad (1)$$

where c_i and \bar{c}_i are respectively the mobile and immobile concentration of a species per unit volume of solution, ω is the porosity, U is the Darcy velocity and D is the hydrodynamic dispersion coefficient (or effective diffusion coefficient when velocity is zero, like in this study). The fixed fraction is evaluated by the chemical calculations, whereas the aqueous fraction is a function of the transport processes. Chemistry and transport are coupled through a sequential iterative algorithm with an adaptive time step. In addition, the HYTEC code is strongly coupled, e.g. the hydrology (flow and diffusion) may change when

mineral precipitation or dissolution changes the local porosity thus allowing to account for clogging in a rigorous manner. A one-dimensional grid of 75 nodes, refined at the cement/claystone interface (grid spacing of 5 cm) was used for the HYTEC calculations presented herein, as shown in Figure 1. Depending on the chemical complexity as discussed below, and for the 100,000 years simulated duration, the CPU time typically ranged from one to five days with a 1,800 GHz processor. Nevertheless, significant reduction of the calculation time can be achieved by using parallel computing techniques. Parallelization of HYTEC is actually under development.

2.2 *Thermodynamic data*

The EQ3/6 thermodynamic database (Wolery, 1992) was selected for the study and enriched with additional data. Table 2 provides all the details regarding the mineral thermodynamic data. “Calcium and silicate hydrate” (CSH) is a generic term that includes a wide variety of poorly crystallized phases of continuous Ca/Si ratio. Three discrete CSH species of increasing Ca/Si ratio, CSH 0.8, CSH 1.1 and CSH 1.8, were introduced to simulate the degradation of the cement phases. Their formation constants were adjusted in order to fit experimental results obtained at 25 °C (Stronach and Glasser, 1997). The cation exchange data, related to the clay minerals, are given in Table 3. Two types of exchange sites were considered: a main site experimentally characterized at the in situ pH (~ 7.7) and a second site in lower concentration but active at higher pH. It has been verified that the model was not significantly sensitive to the uncertainties in the selectivity coefficients. The exchange reactions with $\text{Ca}(\text{OH})^+$ ions were neglected in the calculations due to lack of data.

The calculations of radionuclide solubility and sorption were based on the local equilibrium assumption, and specific data have been introduced for the radionuclides. The thermodynamic constants have been taken from the EQ3/6 database for caesium (Cs) and radium (Ra) and from the NEA database (Rard et al., 1999; Grenthe et al., 1992) for technetium (Tc) and uranium (U). Table 2 summarizes the pure solid phases that are assumed to control the solubility of Ra, Tc and U, according to Berner (1999), Bruno and Sellin (1992) and Glasser (2001). Co-precipitation with CSH and/or sulphoaluminates can occur, but in the absence of thermodynamic data, such a reaction was not considered in the calculations. Disregarding this process is an a priori conservative assumption since co-precipitation usually lowers the radionuclide solubilities. Among the primary and secondary minerals potentially existing in the cement and the claystone, five of them were assumed to play a key role in radionuclide sorption: clinoptilolite, CSH 1.1, CSH 1.8, illite and montmorillonite. Table 3 provides the data used in the calculations. Retention by CSH is commonly modeled

according to the surface complexation theory, whereas cation exchange models are used for clay minerals and zeolites. There are two main types of site for caesium retention by illite (Poinssot et al., 1999): a site of low concentration but very high affinity and a second site of high concentration but lower affinity. Radioactive decay and decay chains are not implemented in HYTEC. However, the decay may be neglected for Cs ($T_{1/2} \text{ } ^{135}\text{Cs} = 2 \times 10^6 \text{ y}$), Tc ($T_{1/2} \text{ } ^{99}\text{Tc} = 2 \times 10^5 \text{ y}$) and the U series over 100,000 years. The half-life of ^{226}Ra is 1,600 years only, but this radionuclide is a permanent product of the $4N+2$ decay chain (^{238}U).

3 Modeling cement-claystone interactions

A rather large variety of precipitated secondary minerals is found in the experimental literature on cement-rock interactions. Dissolution of smectite minerals has been observed (Bauer and Berger, 1998; Hodgekinson and Hughes, 1999; Huertas et al., 2000; Savage et al., 1992), especially for high pH conditions ($\text{pH} \geq 13$) and for moderately high temperatures ($\geq 70 \text{ } ^\circ\text{C}$). Precipitation of C(A)SH, carbonates (e.g. calcite), hydroxides (e.g. brucite, hydrotalcite), sulphates (e.g. ettringite) have almost always been noticed (Adler et al., 1999; Bateman et al., 1999; Hodgekinson and Hughes, 1999; Huertas et al., 2000; Karnland, 1997; Read et al., 2001; Savage et al., 1992; Steefel and Lichtner, 1998). Precipitation of sepiolite, a magnesium phyllosilicate, was observed by Adler (2001) and Read et al. (2001). In the case of fresh cements, as assumed in this study, the high pore water content in potassium can induce the precipitation of illite and/or the illitization of the smectitic clay minerals (Adler et al., 1999; Adler, 2001; Huertas et al., 2000). Concurrently, precipitation of K-feldspar has also been reported (Bauer and Berger, 1998; Chermak, 1993; Hodgekinson and Hughes, 1999) but was not considered in the present paper. In the long term, precipitation of zeolites at low temperature is still a debated question. Zeolites have nevertheless been observed in low contents in experiments or in higher proportions in natural analogues (Bateman et al., 1999; Huertas et al., 2000; Smellie, 1998; Steefel and Lichtner, 1998; Savage et al., 2002). When clay minerals such as illite and smectite are present, ion exchange occurs and influences the overall geochemistry (Adler, 2001; Karnland, 1997).

3.1 Mineralogical evolution

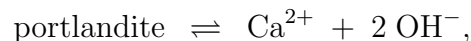
A problematic issue in modeling cement/rock interactions is to select the mineralogical transformations that may occur. Considering the whole set of minerals introduced in the EQ3/6 database generally lead to unrealistic results. Dedicated experiments or literature review have to support the modeling. Ac-

According to the above literature review, three hypotheses specified in Table 4 were introduced in our calculations, from the most consensual to the particular cases. This was done in order to obtain a general trend and to assess the sensitivity of the alkaline plume and the claystone degradation with respect to the experimental variability or uncertainty. The effect of the mineralogical reaction scheme on the alkaline plume buffering was a point of particular interest. Another one was to assess the potential loss of radionuclide containment properties of the multi-barrier system. For instance, the destruction of clay mineral may lead or not to new phases with important retention capability. Since precipitation of CSH, hydroxides and carbonates are almost always observed (for kinetic reasons), the first hypothesis (hyp. A) for calculation is to let only these minerals precipitate during the reactions. Precipitation of illite (or potassic feldspar), commonly observed due to the massive input of potassium ions by Portland cement, is also introduced in hypothesis A. When clay minerals such as illite and smectite are present, ion exchange will occur and influence the overall geochemistry. Therefore, a second hypothesis (hyp. B) is to add this process to the previous calculation. This permits to point out the specific contribution of “sorption” reactions to the alkaline plume buffering. Though less plausible at low temperature for kinetic reasons, precipitation of more crystallized phases than CSH, such as sepiolite and zeolites, and the reformation of montmorillonite (smectitization), were nevertheless considered as a third hypothesis (hyp. C). This last hypothesis also accounts for ion exchange and/or surface complexation for CSH, clay minerals and zeolites (see Table 3).

All simulations were based on the local equilibrium assumption. Although presenting some limitations (Berner, 1998), there are many justifications for a thermodynamic equilibrium approach. The time scales considered are very long, up to 100,000 years, whereas many chemical reactions reach equilibrium within a few months or years: ionic exchange, dissolution/precipitation of carbonates, sulfates, hydroxides and CSH. Furthermore, the chemical gradients between cement and claystone are very strong, speeding up the geochemical reactions. Another reason is that cement and claystone present very high surface/water ratios due to the small pore size. Finally, kinetic data are by nature dependent on the reaction sequence (inhibition or catalyzing effects, etc). These data are not very well characterized and may change during reaction, e.g. with the evolution of the reactive surface. Kinetics were nevertheless indirectly taken into account in the present study through the mineralogical hypotheses of Table 4, which correspond to kinetic inhibitions of secondary mineral precipitation.

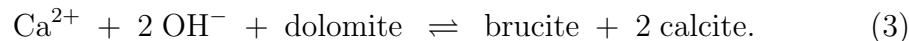
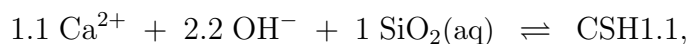
The pH distribution is followed as a key indicator of the degree of mineralogical transformations and the alkaline plume extension, and because it influences sorption and solubility of many elements. Figure 2 provides the pH profiles calculated over a period of 100,000 years for hypotheses A to C in a 1D

configuration. The profile of a non reactive tracer, initially present in the cement zone, is also given for comparison purposes. In the figures, “height” means the vertical direction, towards the upper aquifer. The mass transfer is very slow and decreases with time as expected for diffusive transport. The discontinuities in the curve, especially at 1,000 years, are due to different diffusion coefficients assigned to cement, EDZ-I, EDZ-II and host-rock. In the cement, the pH progressively drops from 13.3 to 12.6, due to diffusion-driven removal of sodium and potassium ions. The pH is then buffered by the dissolution of portlandite and CSH 1.8, successively:



The relation between pH and CSH stability depends on the Ca/Si ratio: the higher the concentration in Ca, the higher the pH of stability. As a result, CSH 1.1 precipitates abundantly at the interface in both the cement and the claystone (Fig. 3). The global evolution of pH, from 13.3 to 10.5 at the interface, is in good agreement with common observations related to cement ageing.

As clearly illustrated by Figure 2, the alkaline plume is buffered close to the interface at a value of 11.5 or below. Farther from the interface, the extension of the attenuated alkaline plume depends on which mineralogical hypothesis is used. Figure 3, representative of hypotheses A and C, explains the origin of this buffering, i.e. mineral dissolution and precipitation. The step-like shape of the mineral concentrations is a consequence of the porosity values assigned to each zone as detailed in Table 1: the higher the porosity, the smaller the concentration of minerals if expressed in moles per liter of pore water. CSH 1.1 and brucite (or hydrotalcite) abundantly precipitate at the interface at the expense of primary cement and claystone minerals, thus controlling pH:



A moderate precipitation of illite, favored by the flux of potassium ions from the cement, also participates to pH buffering. Montmorillonite remains essentially unchanged. Farther from the interface, the combination of dolomite dissolution and calcite precipitation has been experimentally observed and seems specific to claystones and marls (Adler et al., 1999).

For hypothesis C, a second zone of pH buffering is located at the front of montmorillonite transformation into illite and Ca-zeolite. This illitization process is induced by both the flux of potassium ions from the Portland cement and the destabilization of montmorillonite. Sepiolite is more stable than brucite and precipitates close to the interface. Regarding zeolites, scolecite is thermo-

dynamically predicted in simulations, but chabazite, phillipsite or clinoptilolite are more commonly observed (Smellie, 1998). In the present simulations, clinoptilolite was considered as the most representative species due to the availability in literature of radionuclide exchange constants for this mineral. Zeolites are less stable than CSH at the interface where pH and calcium contents are higher.

3.2 Cation exchange processes

In addition to mineral transformations, cation exchange represents a second source of pH buffering. This is shown in Figure 2. The pH profile for hypothesis B is significantly delayed with respect to hypothesis A. The single difference between both assumptions is the integration of cation exchange processes within the type B simulation. Figure 4 helps to explain the relation existing between pH and exchange mechanisms. The alkaline plume leaving the cement does not only raise the concentration of hydroxyl ions (OH^-) but also that of K^+ and, in the long term, Ca^{2+} . A fraction of these cations is retained by the clay minerals according to exchange reactions with the fixed Na^+ and protons. The exchanged protons neutralize the hydroxyl ions and consequently control the alkaline pH as long as the source of exchangeable ions is not depleted. The exchange between aqueous Ca^{2+} and fixed Mg^{2+} contributes to the precipitation of brucite in addition to dolomite dissolution.

3.3 Clogging at the cement/claystone interface

Precipitation of calcite or minerals with a high molar volume, such as CSH and zeolites, may lead to a significant decrease of the pore volume at the cement-claystone interface. Clogging is plausible based on experimental evidences (Adler, 2001) and natural observations (Smellie, 1998). The change in porosity can be calculated by HYTEC from the evolution of the mineral concentrations in the system, knowing their molal volume. The effective diffusion coefficient is then related to the porosity according to Archie's law (Lagneau, 2000). Figure 5 gives an illustration of the clogging process taking into account the feedback of chemistry on transport (a detailed analysis is in preparation by Lagneau et al). Figure 5 corresponds to a zoom at the cement/claystone interface after 2,500 years for hypothesis C. Localized in the claystone, clogging is usually associated with a porosity increase in the cement close to the interface due to portlandite dissolution (see for instance Read et al, 2001). After a transient phase, the cement and claystone subsystems become isolated from each other due to a virtually total sealing of the claystone. Consequently, the diffusion of the high pH plume is strongly reduced, slowing down or even stop-

ping further geochemical evolution of the system. Clogging of the pore space at the cement/claystone interface could be a favorable process for safety, for it limits the perturbation of the geological media and the potential migration of radionuclides (specially for those radionuclides which show no or little sorption). However, this result should be considered with care. The clogged area is relatively thin and thus may be mechanically fragile. The model assumes a homogeneous precipitation within a representative elementary volume and a complete sealing of the pore space. Clogging is more heterogeneously distributed and imperfect in reality.

4 Migration of radionuclides

A direct method to assess the radionuclide mobility is to apply a full mechanistic model which explicitly introduces a radionuclide source in the simulation with ad hoc assumptions on inventory, canister failure, release rate, migration pathway, etc. This method is illustrated in the present paper through the calculation of Cs migration in the context of an early waste package failure just after the resaturation phase. The feedback of chemistry on porosity and diffusion is not introduced in the calculations.

Although Cs is highly soluble, its source term concentration was fixed to the best estimated values of 10^{-5} mol/l from (Berner, 1999) based on ILW inventory. Over 100,000 years, Cs progressively diffuses from the waste into the cement and the clayey host-rock. This is illustrated by Figure 6 for a one-dimensional simulation based on hypothesis C including sorption sites. However, in comparison to the diffusion of a perfect tracer from the waste packages (Fig. 2), the migration of Cs is efficiently delayed by sorption processes (Fig. 6). Cs is retained by CSH in the cement, illite and montmorillonite in the claystone, and zeolite at the interface. The concentrations of all these minerals change with time. At the beginning, the fixed concentration of Cs in the cement is relatively high compared to the claystone since the source is inside the cementitious backfill. The aqueous concentrations are relatively high as well ($\sim 10^{-5}$ mol/l), i.e. the affinity of CSH for Cs is weak. Very low aqueous concentrations ($< 10^{-7}$ mol/l) are calculated in the claystone due to the strong affinity of illite for Cs. At low aqueous Cs concentrations, the sites of high affinity but low density dominate the sorption reaction.

5 Derivation of Kd and solubility limit values

In integrated level transport codes used for performance assessment, each element is transported independently from the others and the full complexity of

chemistry is reduced to a condition on the solubility limit (SL),

$$c_i \leq SL \quad (4)$$

and a single term, Kd_i , the distribution coefficient of element i :

$$Kd_i = \frac{F(c_i)}{c_i} = \frac{\omega}{(1-\omega)\rho_s} \frac{\bar{c}_i}{c_i} \quad (5)$$

The term $F(c_i)$ is the fixed quantity of the element per solid mass (e.g. mol/kg or g/g). The terms c_i and \bar{c}_i are respectively the total aqueous and fixed quantities of the element per unit volume of solution (e.g. mol/m³ or g/ml). In this paper, Kd_i parameters are given in m³/kg units. At last, ρ_s is the density of the solid material (2450 kg/m³ for the Portland cement and 2750 kg/m³ for the host-rock).

Both \bar{c}_i and c_i are mechanistically calculated by HYTEC at any position and any time. Kd and SL values can therefore be calculated based on the results of modeling of cement-claystone interactions. If radionuclides are assumed to be present over the whole domain at any time, SL and Kd profiles can be built. In practice, a calculation without radionuclides is launched and, at predefined times, all the geochemical information needed to calculate the solubility or the aqueous and fixed fractions of an element is saved for each node of the grid. The calculated profiles evolve in time due to the cement/claystone interactions. Their deviation with respect to the constant values used as input data in integrated performance assessment codes can thus be estimated in that way.

5.1 Caesium and radium

Aqueous concentrations have to be fixed in order to calculate the Kd parameter. The previous best estimate value of 10⁻⁵ mol/l was used for the Cs source-term, whereas a concentration of 10⁻⁸ mol/l was set for the Ra source-term; this is slightly below its theoretical maximum solubility for the undisturbed claystone. Figure 7 shows Kd values for Cs calculated in one-dimension for hypothesis C including sorption sites. As already pointed out, the concentrations of the sorbing minerals, and therefore site concentrations, evolve due to the cement/claystone interactions. The initial Kd values calculated with HYTEC are in good agreement with the experimental values of Bradbury and Baeyens (1997a,b) for both cement ($Kd_{Cs} \sim 10^{-3}$ m³/kg) and rocks similar to the reference claystone ($Kd_{Cs} \sim 10^{-1}$ m³/kg). The retention of Cs is much more effective in claystone than in cement due to the high affinity of Cs for illite. Within claystone, the competitive effect with calcium and potassium ions diffusing from cement leads to a decrease in Kd (up to one order of magnitude). However, after 5,000 years of interaction, the formation of

zeolite significantly raises Kd_{Cs} . The Kd decrease in time within the cement is directly related to the re-protonation of silanol type sites of CSH and the increase of calcium concentration due to the pH drop.

Compared to the very long simulated duration, the initial ^{226}Ra inventory will rapidly become negligible due to the relatively short half-life of this nuclide. A direct simulation of Ra migration over this period, as it has been done for Cs, would not be correct. In equilibrium with ^{238}U , ^{226}Ra is nevertheless permanently produced and its presence may contribute to the dosimetric impact of repository on very long-time frames. The potential change of the Kd and SL parameters due to the cement/claystone interactions has been evaluated in this respect. As shown in Figure 7, the initial Kd calculated with HYTEC in the cementitious barrier is higher than the value of $10^{-2} \text{ m}^3/\text{kg}$ reported by Bradbury and Baeyens (1997a). However, the calculated Kd rapidly drops to such a value with decreasing pH and increasing Ca aqueous concentration. In the claystone, the initial Kd calculated with HYTEC is in good agreement with the best experimental estimate of Bradbury and Baeyens (1997b) ($Kd_{Ra} \sim 2.5 \cdot 10^{-2} \text{ m}^3/\text{kg}$). The evolution with time of the Kd_{Ra} profile is similar to the Cs one: decrease in the claystone due to K and Ca competition is significantly compensated, though, by the precipitation of clinoptilolite close to the interface. The SL obtained for Ra in case of hypothesis C is given in Figure 7. This parameter is in agreement with data commonly found in literature for natural media. The claystone pore water is not far from saturation with $RaCO_3$, which may become the limiting phase in more carbonated waters. In the context of this study, the solubility of Ra is only controlled by $RaSO_4$ in both cement and claystone. The aqueous sulfate concentration progressively increases, as shown in Figure 7. This is due to the dissolution of ettringite at the cement/claystone interface. The radium SL decreases accordingly in the cement (from $6 \cdot 10^{-8} \text{ mol/l}$ to $1 \cdot 10^{-8} \text{ mol/l}$).

5.2 Technetium and uranium

The solubilities of many radionuclides, and in particular uranium, are significantly lowered under reducing conditions compared to oxidizing ones. The redox state of common Portland cement is poorly constrained. In the context of waste disposal, low Eh values may be imposed by specific blending additives, e.g. iron blast furnace slag, and/or the corrosion of the steel containers, which leads to magnetite formation. Eh values as low as - 400 mV have been measured in blended Portland cements (Glasser, 2001). Magnetite was used to fix the cement Eh potential in the present calculations. For neutral or slightly alkaline conditions, Eh is controlled by the mineral paragenesis formed by goethite and pyrite (Beaucaire et al., 2000). At higher pH, magnetite and pyrite will dominate. These three minerals were considered in the calculations:

magnetite in the cementitious material, goethite and pyrite in the host-rock. The calculated initial redox potential is -540 mV for cement and -210 mV for the claystone. The redox potential decreases with time in the claystone consequently to the alkaline plume propagation.

The theoretical SL of Tc and U are shown in Figure 8 for hypothesis C. There is initially a difference of more than two orders of magnitude between the theoretical solubility of Tc in cement and claystone pore waters. Uranium is less soluble than technetium. The HYTEC calculations lead to results for Tc and U which are in good agreement with the compilations of Berner (1999) and Bruno and Sellin (1992). For both elements, the solubility is controlled by the balance between complexation with hydroxyl ligands ($\text{Tc}(\text{OH})_3^-$ and $\text{U}(\text{OH})_5^-$ in cement, $\text{Tc}(\text{OH})_2(\text{aq})$ and $\text{U}(\text{OH})_4(\text{aq})$ in claystone) and the precipitation of silicate mineral (coffinite) or oxides ($\text{TcO}_2 \cdot 1.6\text{H}_2\text{O}(\text{s})$, uraninite $\text{UO}_2(\text{s})$), as shown in Figure 8. The choice of $\text{TcO}_2 \cdot 1.6\text{H}_2\text{O}(\text{s})$ is a realistic but rather conservative assumption. The solubility of Tc would be reduced by four orders of magnitude if well crystallized TcO_2 was the controlling phase. The SL decreases with the pH drop inside the cement, whereas the propagation of the attenuated alkaline plume in claystone increases the solubility limits in the EDZ zone by a factor of ten. However, the solubility of technetium, and to a lesser extent of uranium, is very sensitive to the redox potential, Eh. If the redox conditions become less reducing than calculated from the couple goethite/pyrite, Tc and U solubilities will increase significantly in the cement and moderately in the disturbed claystone. For example, at a pH of 12 and an Eh of -250 mV, the dominant redox species are Tc(VII) and U(VI) and the solubilities of Tc and U are about 10^{-4} mol/l and 10^{-6} mol/l respectively.

No Kd values were computed for Tc and U due to lack of thermodynamic sorption data under reducing conditions. Experimental results indicate a high retention of U by cement and rocks similar to the reference claystone; Kd_U values of about $1 \text{ m}^3/\text{kg}$ are reported by Bradbury and Baeyens (1997a) in both materials. Similar values are found in literature for Tc in strongly reducing conditions, but there is no significant Tc retention in mildly reducing and oxidizing conditions.

6 Conclusions

The current progress in reactive transport modeling brings promising application of coupled C-H codes to performance assessment of nuclear repositories. This is especially interesting when assessing near-field evolution where a strong coupling between geochemical and hydrogeological processes is expected. Radionuclide migration can be introduced in the simulations. Theoretical Kd and solubility-limit profiles can be formally calculated, and their sensitivity es-

timated with respect to the system evolution, provided that the corresponding thermodynamic data are available. Indeed, the lack of such data, for instance actinide sorption under reducing conditions, constitutes today a limit to this type of process level modeling.

In the present study, four interdependent mechanisms are shown to control the pH profile in the near-field system: diffusion of the alkaline plume, mineralogical buffering, ion exchange and clogging of the pore space at the cement/claystone interface. After 100,000 years, the pH is partially buffered whatever the mineralogical hypotheses and important mineral transformations occur around the interface, both in cement and host-rock, over only a few meters. However, the destruction of the primary minerals is characterized by the formation of new phases with retention properties (illite, zeolite). Farther in the host-rock, the pore water chemistry is disturbed over some 10 m due to an attenuated but continuous flux of hydroxyl, potassium and calcium ions. Variations of one order of magnitude are calculated for the Kd and the solubility limits of the selected radionuclides (Cs, Ra, Tc and U). This is within the range of commonly found uncertainties on such transport parameters. Nevertheless, this finding cannot be generalized to other radionuclides. Moreover, reactivity of organic matter and Eh poisoning in high pH media are critical aspects, with respect to their potential effect on actinide solubility, which need to be further investigated. At last, work is in progress to simulate in two dimensions other configurations of disposal facilities for so-called altered scenarios, e.g. accounting for advection in addition to diffusion within EDZ, that may change the intensity and expansion of the alkaline perturbation.

Financial support was provided by the French Institute for Radioprotection and Nuclear Safety (IRSN). Fruitful discussions with our colleagues, F. Besnus (IRSN) and V. Lagneau (EMP), and constructive comments of professors F. P. Glasser and L. Moreno are gratefully acknowledged.

References

- Adler, M., 2001. Interaction of claystone and hyperalkaline solutions at 30 °C: a combined experimental and modeling study. Ph.D. thesis, Bern University (Switzerland).
- Adler, M., Mäder, U., Waber, H. N., 1999. High-pH alteration of argillaceous rock : an experimental study. *Schw. Miner. Petr. Mitt.* 79, 445–454.
- Ames, L. L., 1964. Some zeolite equilibria with alkaline metal cations. *Americ. Mineral.* 49, 127–145.
- Bateman, K., Coombs, P., Noy, D. J., Pearce, J. M., Wetton, P., Haworth, A., Linklater, C., 1999. Experimental simulation of the alkaline disturbed zone around a cementitious radioactive waste repository: numerical modelling and column experiments. *Geol. Soc. London* 157, 183.
- Bauer, A., Berger, G., 1998. Kaolinite and smectite dissolution rate in high molar KOH solution at 35 °C and 80 °C. *Appl. Geoch.* 13-7, 905–916.
- Beaucaire, C., Pitsch, H., Toulhoat, P., Motellier, S., Louvat, D., 2000. Regional fluid characterization and modelling of water-rock equilibria in the Boom clay formation and in the Rupelian aquifer at Mol, Belgium. *Appl. Geochem.* 15, 667.
- Berner, U., 1998. Geochemical modelling of repository systems: limitation of the thermodynamic approach. *Radiochim. Acta* 82, 423–428.
- Berner, U., 1999. Concentration limits in the cement based Swiss repository for long-lived, intermediate-level radioactive wastes (LMA). Tech. Rep. 99-10, PSI.
- Bradbury, M. H., Baeyens, B., 1997a. Far-field sorption data bases for performance assessment of a L/ILW repository in an disturbed/altered Palfris marl host rock. Tech. Rep. PSI 97-16, Paul Scherrer Institut, Villigen (CH).
- Bradbury, M. H., Baeyens, B., 1997b. Far-field sorption data bases for performance assessment of a L/ILW repository in an undisturbed Palfris marl host rock. Tech. Rep. PSI 97-15, Paul Scherrer Institut, Villigen (CH).
- Bruno, J., Sellin, P., 1992. Radionuclide solubilities to be used in SKB-91. Tech. Rep. 92-13, SKB.
- Cabrera, J., Volant, P., Baker, C., Pettitt, W., Young, R. P., 1999. Structural and geophysical investigations of the EDZ (Excavation Disturbed Zone) in indurated argillaceous media: the tunnel and the galleries of the IPSN Tournemire site (France). In: *Vail Rocks '99*. Colorado (US).
- Chermak, J. A., 1993. Low temperature experimental investigation of the effect of high pH KOH solutions on the Opalinus shale, Switzerland. *Clays and Clay miner.* 41(3), 365–372.
- Cranga, M., Trotignon, L., Martial, C., Castelier, E., 1998. Simulation of the evolution of a clay engineered barrier by interaction with granitic groundwater: dynamics and characteristics timescales. *Mat. Res. Soc. Symp. Proc.* 506, 629.
- Crovisier, J. L., Fritz, B., Grambow, B., Eberhart, J. P., 1985. Dissolution of basaltic glass in seawater: experiments and thermodynamics modelling.

- Mat. Res. Soc. Symp. Proc. 50, 273.
- De Windt, L., Cabrera, J., Boisson, J.-Y., 1999. Radioactive waste containment in indurated claystones: Comparison between the chemical containment properties of matrix and fractures. Geological Society of London (Special Publication on Chemical Containment of Waste in the Geosphere) , 167–181.
- Glasser, F. P., 2001. Mineralogical aspects of cement in radioactive waste disposal. Mineral. Mag. , 621–633.
- Grenthe, I., Fuger, J., Konings, R. J., Lemire, R. J., Muller, A. B., Nguyen-Trung, C., Wanner, H., 1992. Chemical thermodynamics of uranium. North-Holland, Amsterdam (NL).
- Hodgekinson, E. S., Hughes, C. R., 1999. The mineralogy and geochemistry of cement/rock reactions: high-resolution studies of experimental and analogues materials. Geological Society of London (Special Publication on Chemical Containment of Waste in the Geosphere) , 195–212.
- Huertas, F., Farias, J., Griffault, L., Leguey, S., Cuevas, J., Ramirez, S., Vigil de la Villa, R., Cobena, J., Andrade, C., Alonso, M. C., Hidalgo, A., Parneix, J. C., Rassineux, F., Bouchet, A., Meunier, A., Decarreau, A., Petit, S., Veillard, P., 2000. Effects of cement on clay barrier performance: Ecoclay project. Vol. European Report, EUR 19609 EN.
- Karnland, O., 1997. Cement/bentonite interaction: results from 16 months laboratory experiments. Tech. Rep. 97-32, SKB.
- Lagneau, V., 2000. Influence des processus géochimiques sur le transport en milieu poreux. Ph.D. thesis, École des Mines de Paris (France).
- Lagneau, V., van der Lee, J., in preparation. Simulation of the clogging effects in the near-field of a deep radioactive waste repository: MX80-clay/concrete interface .
- Poinssot, C., Bayens, B., Bradburry, M. H., 1999. Experimental and modelling study of the Cs sorption on illite. Geoch. Cosmoch. Acta 63 (19-20), 3217–3227.
- Rard, J. A., Rand, M. H., Anderegg, G., Wanner, H., 1999. Chemical thermodynamics of technetium. North-Holland, Amsterdam (NL).
- Read, D., Glasser, F. P., Ayora, C., Guardiola, M. P., Sneyers, A., 2001. Mineralogical and microstructural changes accompanying the interaction of Boom Clay with ordinary Portland cement. Adv. Cement Res. 13(4), 175–183.
- Sagar, B., Browning, L., Painter, S., 2002. Coupled transport reaction processes in performance assessment. In: FZK Trepro'02 Workshop, modeling of coupled transport reaction processes, FZK report FZKA 6721. Karlsruhe (D), pp. 73–77.
- Savage, D., 1994. The scientific and regulatory basis for the geological disposal of radioactive waste. John Wiley and Sons, Chichester.
- Savage, D., Bateman, K., Hill, P., Hughes, C., Milodowski, A., Pearce, J., Rae, E., Rochelle, C., 1992. Rate and mechanism of the reaction of silicates with cement pore fluids. Applied Clay Sc. 7, 33.
- Savage, D., Noy, D., Mihara, M., 2002. Modelling the interaction of bentonite

- with hyperalkaline fluids. *Appl. geoch.* 17, 207–223.
- Smellie, J. A. T., 1998. Maqarin natural analogue study: phase III. Tech. Rep. 98-04, SKB.
- Steeffel, C. I., Lichtner, P. C., 1998. Multicomponent transport in discrete fractures. II : Infiltration of hyperalkaline groundwater at Maqarin, Jordan, a natural analogue site. *J. of Hydrology* 209, 200–224.
- Stronach, S. A., Glasser, F. P., 1997. Modeling the impact of abundant geochemical components on phase stability and solubility of the CaO-SiO₂-H₂O systems at 25 °C: Na⁺, K⁺, SO₄²⁻, Cl⁻ and CO₃²⁻. *Adv. Cement. Res* 9, 167–181.
- van der Lee, J., De Windt, L., 2001. Present state and future directions of modeling geochemistry in hydrogeological systems. *J. Cont. Hydr.* 47, 265–282.
- van der Lee, J., De Windt, L., Lagneau, V., Goblet, P., 2003. Module-oriented modeling of reactive transport with HYTEC. *Comp. Geosc* 29, 265–275.
- Viallis-Terrisse, 2000. Interaction des silicates de calcium hydratés, principaux constituants du ciment, avec les chlorures d'alcalins. Analogie avec les argiles. Ph.D. thesis, Université de Bourgogne (France).
- Wolery, T., 1992. EQ3/6. A software package for geochemical modelling of aqueous systems: package overview and installation guide (version 7.0). Tech. Rep. UCRL-MA-110662 PT I ed., Lawrence Livermore National Laboratory, USA.

Table 1
Hydrogeological parameters.

	Porosity	D_p (m ² /s)	D_{eff} (m ² /s)
Cement	0.20	$1.0 \cdot 10^{-10}$	$2.0 \cdot 10^{-11}$
Host-rock	0.15	$1.0 \cdot 10^{-10}$	$1.5 \cdot 10^{-11}$
EDZ-I	0.35	$1.0 \cdot 10^{-9}$	$3.5 \cdot 10^{-10}$
EDZ-II	0.20	$2.5 \cdot 10^{-10}$	$5.0 \cdot 10^{-11}$

Table 2. Reactions and equilibrium constants for minerals.

Mineral	Reaction	LogK		Ref.
		0 °C	25 °C	
Brucite	$\text{Mg}^{2+} + 2\text{H}_2\text{O} \rightarrow \text{Mg}(\text{OH})_2 + 2\text{H}^+$	-18.09	-16.30	[1]
Calcite	$\text{Ca}^{2+} + \text{HCO}_3^- \rightarrow \text{CaCO}_3 + \text{H}^+$	-2.23	-1.85	[1]
Clinoptilolite	$1.75\text{Ca}^{2+} + 3.5\text{Al}^{3+} + 14.5\text{SiO}_2(\text{aq}) + 18\text{H}_2\text{O} \rightarrow$ $\text{Ca}_{1.75}\text{Al}_{3.5}\text{Si}_{14.5}\text{O}_{36} \cdot 11\text{H}_2\text{O} + 14\text{H}^+$	7.34	7.01	[1]
Coffinite	$\text{U}^{4+} + \text{SiO}_2(\text{aq}) + 2\text{H}_2\text{O} \rightarrow \text{USiO}_4 + 4\text{H}^+$	7.32	8.05	[4]
CSH 0.8	$0.8\text{Ca}^{2+} + \text{SiO}_2(\text{aq}) + 1.6\text{H}_2\text{O} \rightarrow \text{CSH } 0.8 + 1.6\text{H}^+$	-	-11.07	[2]
CSH 1.1	$1.1\text{Ca}^{2+} + \text{SiO}_2(\text{aq}) + 2.2\text{H}_2\text{O} \rightarrow \text{CSH } 1.1 + 2.2\text{H}^+$	-	-16.69	[2]
CSH 1.8	$1.8\text{Ca}^{2+} + \text{SiO}_2(\text{aq}) + 3.6\text{H}_2\text{O} \rightarrow \text{CSH } 1.8 + 3.6\text{H}^+$	-	-32.58	[2]
Dolomite	$\text{Ca}^{2+} + \text{Mg}^{2+} + 2\text{HCO}_3^- \rightarrow \text{CaMg}(\text{CO}_3)_2 + 2\text{H}^+$	-3.41	-2.51	[1]
Etringite	$2\text{Al}^{3+} + 6\text{Ca}^{2+} + 3\text{SO}_4^{2-} + 38\text{H}_2\text{O} \rightarrow \text{Ca}_6\text{Al}_2(\text{SO}_4)_3(\text{OH})_{12} \cdot 26\text{H}_2\text{O} + 12\text{H}^+$	-68.98	-62.54	[1]
Goethite	$\text{Fe}^{3+} + 2\text{H}_2\text{O} \rightarrow \text{FeO}(\text{OH}) + 3\text{H}^+$	-1.52	-0.53	[1]
Hydrotalcite	$2\text{Al}^{3+} + 6\text{Mg}^{2+} + \text{HCO}_3^- + 16\text{H}_2\text{O} \rightarrow \text{Mg}_6\text{Al}_2\text{CO}_3(\text{OH})_{16} + 17\text{H}^+$	-	-99.56	[3]
Illite	$2.3\text{Al}^{3+} + 0.6\text{K}^+ + 0.25\text{Mg}^{2+} + 3.5\text{SiO}_2(\text{aq}) + 5\text{H}_2\text{O} \rightarrow$ $\text{K}_{0.6}\text{Mg}_{0.25}\text{Al}_{2.3}\text{Si}_{3.5}\text{O}_{10}(\text{OH})_2 + 8\text{H}^+$	-11.39	-9.03	[1]
Kaolinite	$2\text{Al}^{3+} + 2\text{SiO}_2(\text{aq}) + 5\text{H}_2\text{O} \rightarrow \text{Al}_2\text{Si}_2\text{O}_5(\text{OH})_4 + 6\text{H}^+$	-9.02	-6.81	[1]
Magnetite	$\text{Fe}^{2+} + 2\text{Fe}^{3+} + 4\text{H}_2\text{O} \rightarrow \text{Fe}_3\text{O}_4 + 8\text{H}^+$	-13.90	-10.47	[1]
Montmorillonite	$1.67\text{Al}^{3+} + 0.165\text{Ca}^{2+} + 0.33\text{Mg}^{2+} + 4\text{SiO}_2(\text{aq}) + 4\text{H}_2\text{O} \rightarrow$ $\text{Ca}_{0.165}\text{Mg}_{0.33}\text{Al}_{1.67}\text{Si}_4\text{O}_{10}(\text{OH})_2 + 6\text{H}^+$	-3.67	-2.50	[1]
Natrolite	$2\text{Al}^{3+} + 2\text{Na}^+ + 3\text{SiO}_2(\text{aq}) + 6\text{H}_2\text{O} \rightarrow \text{Na}_2\text{Al}_2\text{Si}_3\text{O}_{10} \cdot 2\text{H}_2\text{O} + 8\text{H}^+$	-21.21	-18.52	[1]
Portlandite	$\text{Ca}^{2+} + 2\text{H}_2\text{O} \rightarrow \text{Ca}(\text{OH})_2 + 2\text{H}^+$	-	-22.82	[2]
Pyrite	$\text{Fe}^{2+} + 1.75\text{HS}^- + 0.25\text{SO}_4^{2-} + 0.25\text{H}^+ \rightarrow \text{FeS}_2 + \text{H}_2\text{O}$	26.50	24.65	[1]
Quartz	$\text{SiO}_2(\text{aq}) \rightarrow \text{SiO}_2$	4.63	4.00	[1]
RaCO ₃	$\text{Ra}^{2+} + \text{HCO}_3^- \rightarrow \text{RaCO}_3 + \text{H}^+$	3.29	3.00	[1]
RaSO ₄	$\text{Ra}^{2+} + \text{SO}_4^{2-} \rightarrow \text{RaSO}_4$	11.18	10.45	[1]
Scolecite	$2\text{Al}^{3+} + \text{Ca}^{2+} + 3\text{SiO}_2(\text{aq}) + 7\text{H}_2\text{O} \rightarrow \text{CaAl}_2\text{Si}_3\text{O}_{10} \cdot 3\text{H}_2\text{O} + 8\text{H}^+$	-18.84	-15.88	[1]
TcO ₂ (c)	$\text{TcO}^{2+} + \text{H}_2\text{O} \rightarrow \text{TcO}_2 + 2\text{H}^+$	-	8.40	[5]
TcO ₂ :1.6H ₂ O(s)	$\text{TcO}^{2+} + 2.6\text{H}_2\text{O} \rightarrow \text{TcO}_2 \cdot 1.6\text{H}_2\text{O} + 2\text{H}^+$	-	4.40	[5]
Uraninite	$\text{U}^{4+} + 2\text{H}_2\text{O} \rightarrow \text{UO}_2 + 4\text{H}^+$	3.57	4.84	[4]

[1] Wolery (1992), [2] Stronach and Glasser (1997), Lagneau (2000), [3] Crovisier et al. (1985), [4] Grenthe et al. (1992), [5] Rard et al. (1999).

Table 3
Surface complexation and ion exchange data.

Mineral	Equation	LogK (25 °C)
CSH [1]	$\equiv\text{CSH-OH} \rightarrow \equiv\text{CSH-O}^- + \text{H}^+$	-12.3
	$\equiv\text{CSH-OH} + \text{Na}^+ \rightarrow \equiv\text{CSH-ONa} + \text{H}^+$	-12.1
	$\equiv\text{CSH-OH} + \text{Ca}^{2+} \rightarrow \equiv\text{CSH-Ca}^+ + \text{H}^+$	-9.4
	$\equiv\text{CSH-OH} + \text{Cs}^+ \rightarrow \equiv\text{CSH-OCs} + \text{H}^+$	-11.3
	$\equiv\text{CSH-OH} + \text{Ra}^{2+} \rightarrow \equiv\text{CSH-Ra}^+ + \text{H}^+$	-9.4
	Site density $\equiv\text{CSH-OH} = 8 \mu\text{mol/m}^2$	
Clinoptilolite [2]	$\text{K}^+ + \overline{\text{Na}} \rightarrow \text{Na}^+ + \overline{\text{K}}$	1.1
	$\text{Ca}^{2+} + 2 \overline{\text{Na}} \rightarrow 2 \text{Na}^+ + \overline{\text{Ca}}$	-0.1
	$\text{Cs}^+ + \overline{\text{Na}} \rightarrow \text{Na}^+ + \overline{\text{Cs}}$	1.7
	$\text{Ra}^{2+} + 2 \overline{\text{Na}} \rightarrow 2 \text{Na}^+ + \overline{\text{Ra}}$	0.1
	CEC = 250 meq/100g	
Illite - Montmorillonite	Main site (90 % CEC) [3]	
	$\text{K}^+ + \overline{\text{Na}} \rightarrow \text{Na}^+ + \overline{\text{K}}$	0.8
	$\text{Ca}^{2+} + 2 \overline{\text{Na}} \rightarrow 2 \text{Na}^+ + \overline{\text{Ca}}$	0.7
	$\text{Mg}^{2+} + 2 \overline{\text{Na}} \rightarrow 2 \text{Na}^+ + \overline{\text{Mg}}$	0.5
	$\text{Cs}^+ + \overline{\text{Na}} \rightarrow \text{Na}^+ + \overline{\text{Cs}}$	2.0
	$\text{Ra}^{2+} + 2 \overline{\text{Na}} \rightarrow 2 \text{Na}^+ + \overline{\text{Ra}}$	0.7
	Secondary site (9-10 % CEC) [4]	
	$\text{H}^+ + \overline{\text{Na}} \rightarrow \text{Na}^+ + \overline{\text{H}}$	7.0
	$\text{Ca}^{2+} + 2 \overline{\text{Na}} \rightarrow 2 \text{Na}^+ + \overline{\text{Ca}}$	1.0
	Strong affinity site for Cs (1 % CEC of illite) [3]	
	$\text{Cs}^+ + \overline{\text{Na}} \rightarrow \text{Na}^+ + \overline{\text{Cs}}$	5.0
	CEC - Illite = 30 meq/100g	
	CEC - Montmorillonite = 90 meq/100g	

Notes: [1] Viallis-Terrisse (2000), Ra approximated by Ca, specific surface = 50 m²/g in our calculations; [2] Ames (1964), Ra approximated by Sr; [3] De Windt et al. (1999) for major ions, Ra approximated by Sr, Poinssot et al. (1999) for Cs (strong affinity site only for illite); [4] Cranga et al. (1998).

Table 4
 Mineralogical hypotheses considered in the simulations.

	Non clay minerals*	Clay minerals
Hyp. A	CSH	illite = equilibrium, smectite = dissolution only
Hyp. B	CSH & cation exch./surf. complex.	illite = equilibrium, smectite = dissolution only
Hyp. C	CSH + sepiolite + zeolites & cation exch./surf. complex.	illite & smectite = equilibrium

*Carbonates, hydroxides, oxides and sulfates are in equilibrium for all hypotheses.

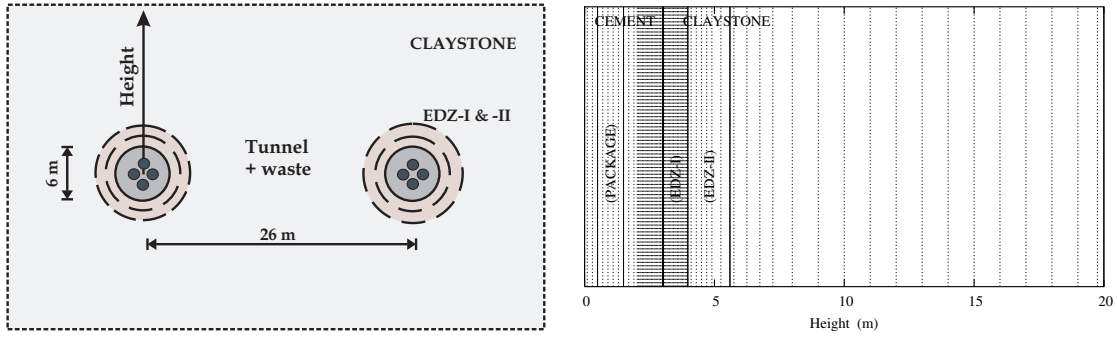


Fig. 1. Schematic 2D vertical cross section of the horizontal tunnels (left) and 1D grid used in the calculations with location of cement, waste package, EDZ and claystone zones (right). In the figures, “height” means the vertical direction, towards the upper aquifer.

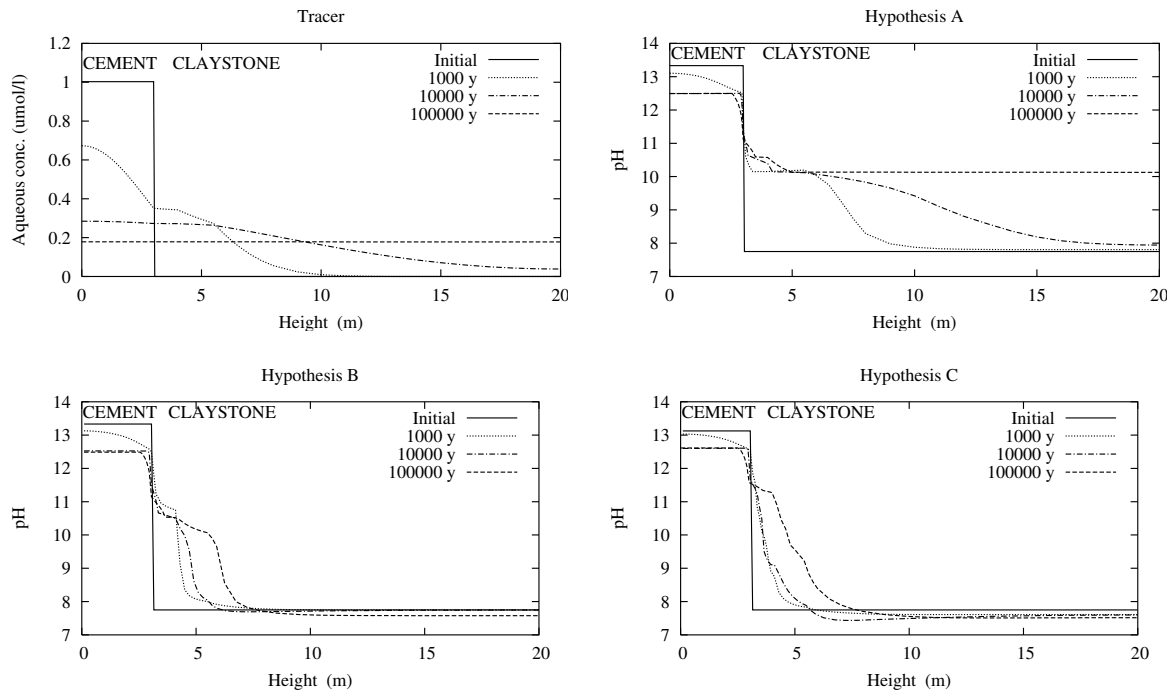


Fig. 2. Evolution over a period of 100,000 years: profiles of the unreactive tracer concentration and profiles of pH for the different mineralogical hypotheses.

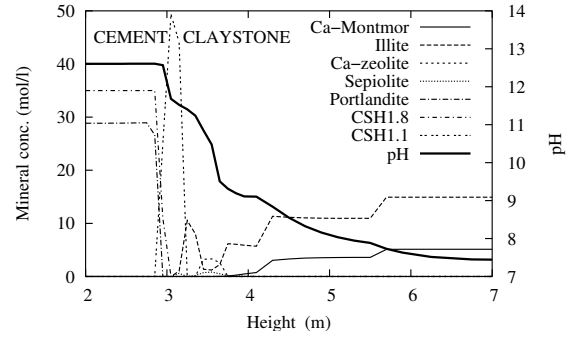
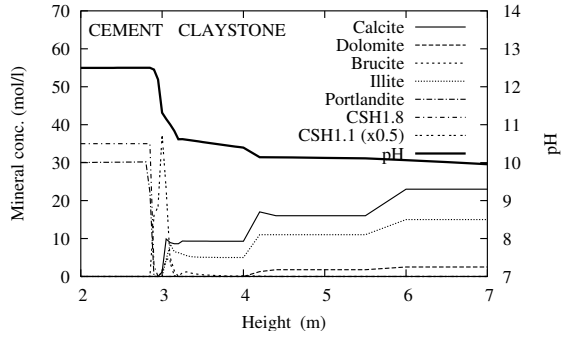


Fig. 3. Mineralogical fronts and related pH profiles after 10,000 years at the interface and within the claystone for hypotheses A (left) and C (right).

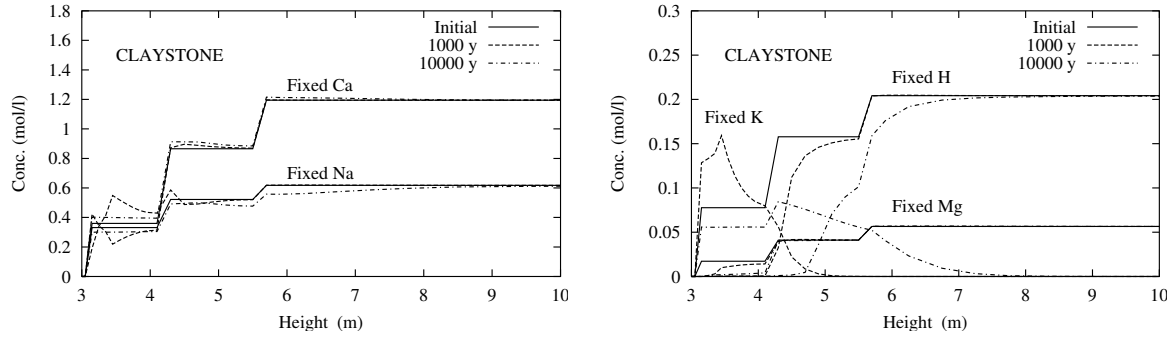


Fig. 4. Evolution of exchangeable ion concentrations over a period of 10,000 years for hypothesis B.

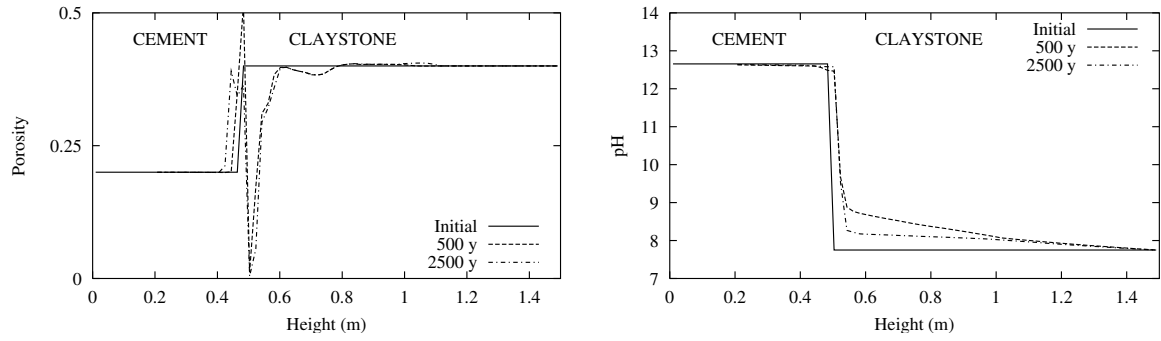


Fig. 5. Zoom at the interface: a strong decrease of the porosity stops the alkaline plume propagation (hypothesis C).

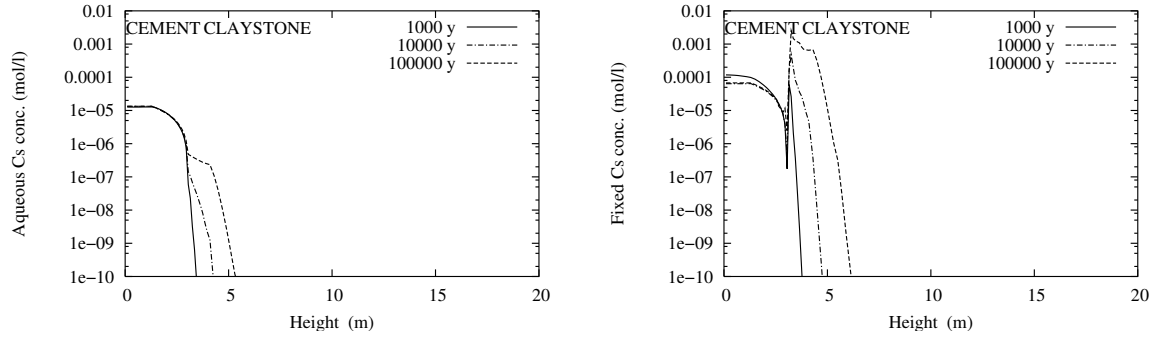


Fig. 6. Evolution of the aqueous and fixed fractions of Cs during its migration from the waste canisters.

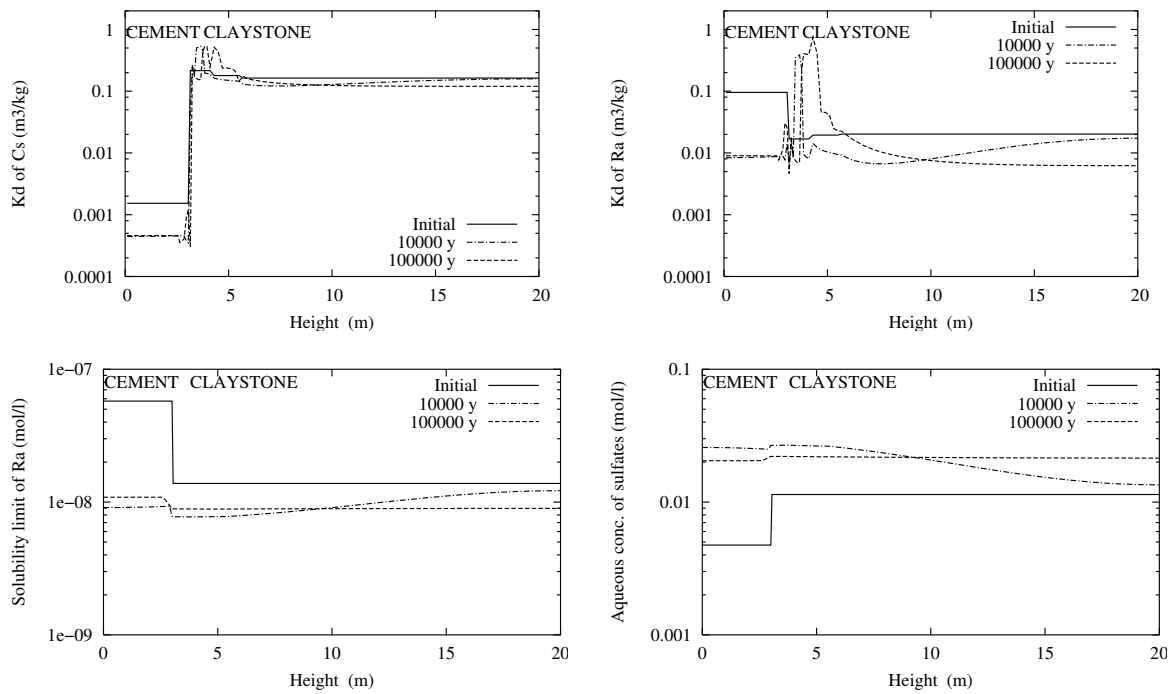


Fig. 7. Derivation of Kd profiles for Cs and Ra and SL profiles for Ra (hypothesis C). Sulfate aqueous concentration controls Ra solubility.

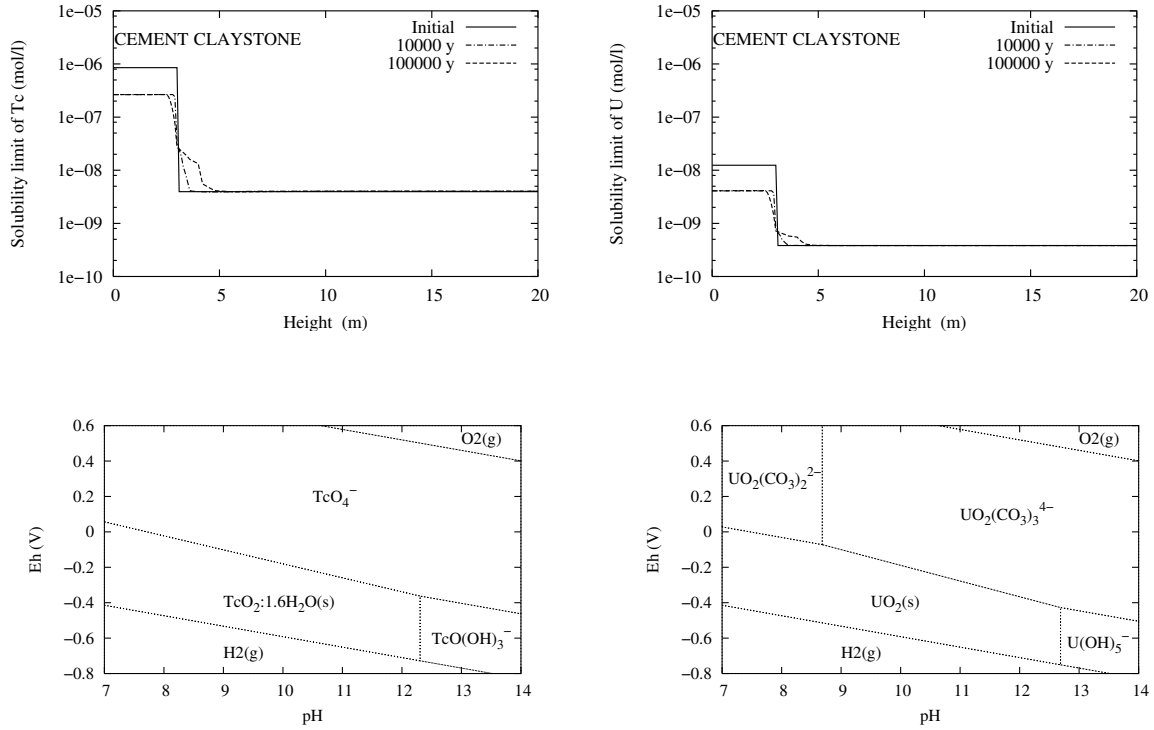


Fig. 8. Derivation of solubility limits for Tc and U (hypothesis C, with redox) and solubility diagrams for Tc and U calculated according to the NEA database (Eh = -0.3 V, T= 20 °C, $[\text{HCO}_3^-] = 1\text{e-}3$, $[\text{Tc}] = 1\text{e-}7$, $[\text{U}] = 1\text{e-}8$).